Energy Storage Materials 49 (2022) 219–226

Contents lists available at ScienceDirect

Energy Storage Materials

journal homepage: www.elsevier.com/locate/ensm

Three-dimensional networking binders prepared *in situ* during wet-slurry process for all-solid-state batteries operating under low external pressure

Tae Young Kwon[a,b], Kyu Tae Kim[a], Dae Yang Oh[a], Yong Bae Song[a], Seunggoo Jun[a], Yoon Seok Jung[a,*]

[a] Department of Chemical and Biomolecular Engineering, Yonsei University, 50 Yonsei-ro, Seodaemun-gu, Seoul 03722, South Korea
[b] Department of Energy Engineering, Hanyang University, Seoul 04763, South Korea

ARTICLE INFO

Keywords:
Solid-state batteries
Sulfide solid electrolytes
Composite electrodes
Slurry processes
In situ crosslinking binders

ABSTRACT

For all-solid-state Li batteries (ASLBs), the external operating pressure offsets the detrimental electrochemo-mechanical effects. In this work, a new scalable *in situ* protocol to reinforce binders for sulfide-electrolyte-based ASLBs operating under low or no external pressures is reported. The vulcanization of butadiene rubber (BR) using elemental sulfur proceeds *in situ* during the wet-slurry fabrication process for electrodes, forming a mechanically resilient crosslinked structure. The electrochemical performance of $LiNi_{0.70}Co_{0.15}Mn_{0.15}O_2$ electrodes fabricated using pristine or vulcanized BR diverge significantly as the operating pressure is lowered from 70 MPa to a practically acceptable value of 2 MPa. Complementary analysis using cross-sectional scanning electron microscopy and operando electrochemical pressiometry measurements confirms that the vulcanization of BR suppresses the electrochemo-mechanical degradation of electrodes, which suggests that the scaffolding structure of the vulcanized BR helps maintain the microstructural integrity of the electrodes upon charge and discharge. The significantly enhanced performance of the vulcanized BR is also demonstrated for pouch-type $LiNi_{0.70}Co_{0.15}Mn_{0.15}O_2/Li_4Ti_5O_{12}$ full cells operated under no external pressure (reversible capacity of 121 vs. 150 mA h g^{-1} at 0.2C for electrodes with pristine vs. vulcanized BR, respectively).

1. Introduction

All-solid-state Li or Li-ion batteries (ASLBs) employing non-flammable inorganic solid electrolytes (SEs) are one of the most promising next-generation rechargeable batteries [1–10]. This is a consequence of the progress in novel inorganic superionic conductors, such as sulfides (e.g., $Li_{5.5}PS_{4.5}Cl_{1.5}$: [11] 10 mS cm^{-1}), oxides (e.g., $Li_7La_3Zr_2O_{12}$: [12] 0.5 mS cm^{-1}), and halides (e.g., Li_3YCl_6: [13,14] 0.5 mS cm^{-1}), toward overcoming the limited safety and energy density issues of conventional lithium-ion batteries [1–4,7,8,15,16]. Despite the extensive progress in ASLB research, technologies for large-scale ASLBs have remained at infancy. In most previous studies, lab-scale pellet-type all-solid-state cells were fabricated with or without polymeric binders [1,2,14,17–21]. Furthermore, they have been tested under high external pressures of tens of megapascal, which is unrealistic for practical applications [1,2,14,17–20,22,23]. Therefore, studies on ASLBs that are operable under no or low external pressure are required to bridge the performance gap between lab-scale test cells and practical cells [7,22,24–26].

Owing to the incompressible and nonflowing features of SEs, electrochemo-mechanical effects are critical to the performance of ASLBs (Fig. 1) [26–34]. While constructing electronic and ionic conduction pathways throughout electrodes is important [35,36], even small volumetric strains of a few to approximately ten percent of cathode active materials (CAMs) during charge and discharge induce the formation of void spaces at the interfaces between the CAM and the SE, and the pulverization of the CAM particle itself [26,29,32,37,38]. Moreover, the volumetric strains upon repeated cycling could degrade the mechanical integrity at the interfaces between the electrode and the SE layers [27,37,38]. Our group also identified an overlooked electrochemo-mechanical degradation mode caused by the decomposition of SEs ($Li_6PS_5Cl_{0.5}Br_{0.5}$ (LPSX)) [29]. All the aforementioned cases indicate the loss and/or loosening of ionic contacts and, in turn, a performance degradation. Notably, these electrochemo-mechanical effects become much more significant under lower external pressures, that is, less than a few megapascal, for practical ASLBs [22,39].

Soft polymeric binders are indispensable components in the fabrication of sheet-type electrodes and SE membranes for large-format ASLBs [18,21,23,40–48]. Moreover, they play a key role in maintaining the microstructural integrity of electrodes during repeated charge–discharge cycles even though they occupy a very small fraction of electrodes

* Corresponding author.
E-mail address: yoonsjung@yonsei.ac.kr (Y.S. Jung).

https://doi.org/10.1016/j.ensm.2022.04.017
Received 20 December 2021; Received in revised form 14 March 2022; Accepted 8 April 2022
Available online 10 April 2022

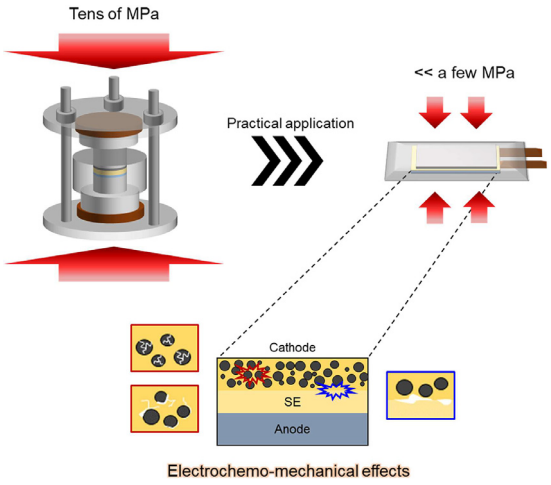

Fig. 1. Schematic illustrating ASLB cells operating under a low pressure (< a few MPa) for practical applications, where the electrochemo-mechanical effects become more pronounced.

[23,45]. Polymeric binders hold the inorganic components together, helping maintain the electronic and ionic contacts upon cycling. Therefore, reinforcing the mechanical properties of polymeric binders is an effective method for buffering the electrochemo-mechanical degradation [49,50]. Moreover, considering the Li^+-insulating property of binders, the fraction of binders can be minimized by enhancing their mechanical properties, which leads to less Li^+ obstruction [23,41,51].

For the fabrication of sheet-type electrodes using sulfide SEs, wet-slurry fabrication is highly complicated owing to the poor chemical stability of sulfide SEs toward processing solvents [23,40,41,46,47]. Thus, highly polar solvents that have been widely used for conventional lithium-ion batteries, such as N-methyl pyrrolidinone, are not suitable for this purpose. Instead, solvents with low or intermediate polarity, such as xylene, dibromomethane, butyl butyrate, and benzyl acetate, have been employed [23,40,41]. Accordingly, rubber-based polymers (e.g., butadiene rubber (BR)) that can be well dissolved (or dispersed) in those solvents have been employed [23,40,41,46,47,52]. In this regard, a strategy to enhance the mechanical properties of rubber-based polymers is necessary for fabricating practical ASLBs employing sulfide SEs.

Herein, we report a new scalable protocol for the *in situ* crosslinking of BR using elemental sulfur, that is, vulcanization, during the wet-slurry fabrication process for sheet-type electrodes employing sulfide SEs. The vulcanization of BR remarkably improves the elastic properties. $LiNi_{0.70}Co_{0.15}Mn_{0.15}O_2$ (NCM) electrodes using vulcanized BR significantly outperform those using pristine BR under a lower operating pressure. The first discharge capacities for the electrodes prepared using vulcanized and pristine binders are 165 and 151 mA h g^{-1} at 2 MPa (0.1C and 30 °C), respectively, which is in contrast to the marginal difference under conventional higher operating pressures (172 vs. 171 mA h g^{-1} at 70 MPa, respectively). Complementary analysis using field-emission scanning electron microscopy backscattered electron (FESEM-BSE) and operando electrochemical pressiometry measurements reveals the suppressed electrochemo-mechanical degradation of the electrodes, enabled by using the crosslinked network polymers.

2. Results and discussion

Vulcanization is a crosslinking process in which individual molecules of rubber are converted into a three-dimensional (3D) network of interconnected chains through chemical crosslinks [53]. BR was vulcanized *in situ* by simply adding elemental sulfur with additives to slurries (Fig. 2a). After casting a slurry containing CAM (NCM), SE (LPSX), a carbon additive (Super C65), BR, sulfur, and additives, vulcanization proceeded during the heat treatment process (drying process). Through vulcanization, the C=C double bonds in the BR chains break, and the sulfur linkages connect the chains with other chains. The resulting 3D network structure of vulcanized BR is different from that of pristine BR with a linear structure, and its physical properties depend on the crosslinking density and efficiency [54]. The crosslinking density indicates the density of chains or segments that connect two infinite parts of the polymer network [55]. The crosslinking efficiency is determined by the ratio of sulfur to the accelerator (2-mercaptobenzothiazole (MBT)). When the sulfur/accelerator ratio varies, the type of sulfidic crosslinking varies and influences the physical properties of the product polymers. Sulfidic linkages in vulcanization systems are classified into monosulfidic (C-S-C), disulfidic (C-S-S-C), and polysulfidic (C-S_x-C) bonds. The fraction of polysulfidic bonds increases as the sulfur/accelerator ratio increases. Three vulcanized BR samples were prepared by varying the sulfur/accelerator ratio: S1 (1 parts per hundred of rubber (phr) sulfur/3 phr MBT), S2 (2 phr sulfur/2 phr MBT), and S3 (3 phr sulfur/1 phr MBT). The measurement of the crosslinking density via a solvent swelling method for all the three samples showed similar values (Fig. 2b) [56]. Raman spectroscopy measurements were conducted to probe the sulfidic linkages (Figs. 2c, d, and S1). In Fig. 2c, the peaks for the polysulfidic and disulfidic bonds are distinct at 440 and 505 cm^{-1}, respectively [57]. Their intensities were normalized and are presented in Fig. 2d. The increased amount of polysulfidic bonds with increasing sulfur/accelerator ratio (from S1 to S3) was confirmed.

The physical properties of the vulcanized BR binders were assessed via tensile (Fig. 2e, f) and nanoindentation tests (Fig. 2g, h). The tensile test results confirmed that the elastic properties of BR could be significantly improved by vulcanization (Fig. 2e and f). Specifically, toughness of the vulcanized BR (S2) was much higher (220 kJ m^{-3}) compared to that of the pristine BR (19 kJ m^{-3}). The nanoindentation results indicated that both the modulus and hardness decreased as the sulfur/accelerator ratio increased (from S1 to S3). Considering the similar crosslinking densities among the three samples (Fig. 2b), this result indicates that the factor governing the physical properties of the vulcanized BR is the crosslinking efficiency rather than the crosslinking density. A higher modulus is desirable to maintain the integrity of the composite electrodes. However, a higher hardness is not directly interpreted as an advantage [58,59]. Thus, the physical performances of the vulcanized binders cannot be arranged easily in order without testing the electrochemical performance, which is discussed further later.

The adaptability of the vulcanized binders for the wet-slurry process using LPSX was assessed by measuring the Li^+ conductivities at 30 °C and obtaining the corresponding X-ray diffraction (XRD) patterns for binder–LPSX composite samples (Table S1, Figs. S2 and S3), which showed a marginal degradation. The NCM electrodes tailored using vulcanized binders (S2) also showed no cracks or delamination (Fig. S4). Moreover, cyclic voltammetry test results showed no significant changes in the electrochemical stability of the binders after vulcanization (Fig. S5).

Electrochemical characterization results at 30 °C for the NCM electrodes with pristine BR (with linear chains) and vulcanized BR (S3, S2, S1, with 3D networks) are shown in Fig. 3. Cross-sectional time-of-flight secondary ion mass spectrometry (TOFSIMS) results in Fig. S6 showed no noticeable differences in binder distribution between electrodes with pristine and vulcanized BR (S2). The first-cycle charge–discharge voltage profiles for NCM/Li-In all-solid-state half cells tested at the operating pressures of 70, 7, and 2 MPa are shown in Fig. 3a. A slight difference in performance was observed at the highest pressure of 70 MPa. However, as the operating pressure was lowered to 7 and 2 MPa, the performance difference became distinct. At 2 MPa, the first-cycle discharge capacity of the electrodes with pristine BR was 151 mA h g^{-1}, which was 20 mA h g^{-1} lower than that at 70 MPa. In contrast, the NCM electrodes with vulcanized BR (S2) showed a first-cycle discharge capacity of 165 mA h g^{-1} at 2 MPa, which was only 7 mA h g^{-1} lower than that at 70 MPa. The

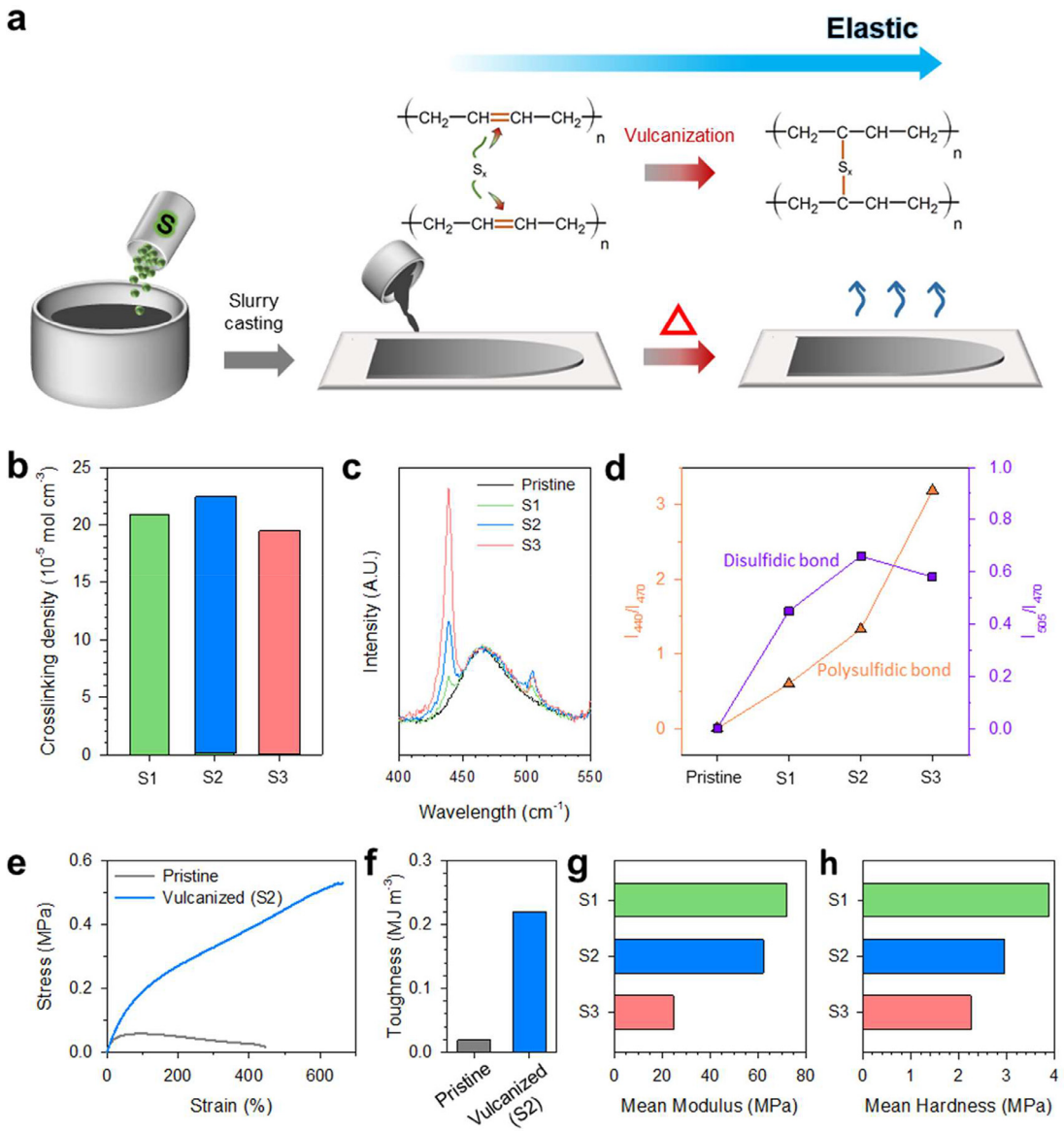

Fig. 2. Results of vulcanized BR (butadiene rubber) binders. (a) Schematic of the *in situ* formation of vulcanized BR binders during the slurry fabrication process for sheet-type electrodes. (b) Crosslinking density of vulcanized BR. (c) Raman spectra and (d) corresponding normalized peak intensities of sulfidic bonds for pristine and vulcanized BR. (e) Stress–strain curves and (f) corresponding toughness for pristine and vulcanized BR. (g) Modulus and (h) hardness of vulcanized BR obtained from the nanoindentation tests.

best performance of the electrodes using S2 among the three samples is understood by considering the physical properties obtained from the nanoindentation tests (Fig. 2g, h). An excessively high hardness may indicate that the electrodes are brittle and prone to breakage before buffering electrochemo-mechanically induced stresses [58,59]. Thus, S2 is considered to possess optimal physical properties in terms of both modulus and hardness. Fig. 3b and c show the first- and subsequent-cycle (2nd- and 3rd-cycle) Coulombic efficiencies for the electrodes using pristine and vulcanized (S2) BR, respectively. The differences between the two electrodes became much larger at lower pressures (Fig. 3b and c). The trend of the considerably better performance with the use of vulcanized BR than with the use of pristine BR at lower applied pressures is also consistent with the rate capability and cycle retention results (Figs. S7–S9). When comparing the discharge voltage profiles for each rate at 2 MPa (Fig. 3d), at higher C-rates, electrodes using vulcanized BR (S2) outperformed those using pristine BR more significantly (e.g., 85 vs. 51 mA h g^{-1} at 1C for the electrodes using vulcanized and pristine BR, respectively). In summary, the electrochemical performance results manifest that the detrimental electrochemo-mechanical effects become more pronounced at lower pressures but can be addressed by using *in situ* vulcanized binders. In addition, half cells using vulcanized binders tested at an elevated temperature of 60 °C were operated without any problems concerning thermally driven (electro)chemical side reactions (Fig. S10).

To assess the mechanical properties of electrodes, affected by the vulcanization of binders, nanoindentation tests were carried out using control sample electrodes comprised of NCM and binders (Fig. S11). The NCM electrodes with S2 exhibited a much higher compressive strength of 34.8 MPa (Fig. S11b), compared to the electrodes with pristine BR (10.1 MPa). This result confirms the enhanced mechanical properties by the vulcanization. Furthermore, the elastic recovery of the NCM electrodes with S2 was higher than that for using pristine BR (Fig. S11c), indicating that the electrodes fabricated using vulcanized BR effectively absorb mechanical stress.

The pressure changes for the NCM electrodes using pristine and vulcanized BR were monitored in real time during charging and discharging

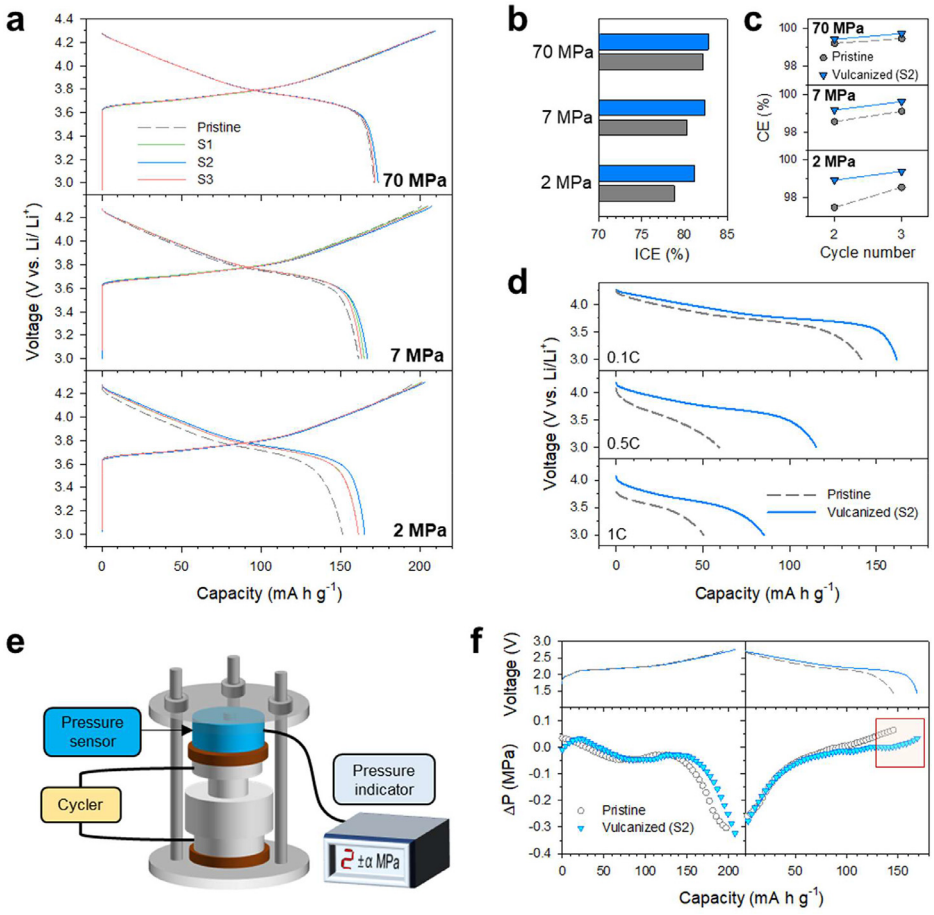

Fig. 3. Comparative electrochemical characterization of sheet-type NCM electrodes fabricated using pristine and vulcanized BR. (a) First-cycle charge–discharge voltage profiles of NCM/Li-In half cells (0.1C and 30 °C) using NCM electrodes with pristine or vulcanized BR under varying operating pressures (70, 7, and 2 MPa). Corresponding (b) initial Coulombic efficiencies (ICEs), (c) Coulombic efficiencies (CEs) at 2nd and 3rd cycles, and (d) discharge voltage profiles at 2 MPa and various C-rates. (e) Schematic of pressure-monitoring all-solid-state cells. Zero-strain LTO was used for the counter electrodes. (f) First-cycle charge–discharge voltage profiles and corresponding pressure changes for NCM electrodes using pristine and vulcanized BR. The high terminal pressure for electrodes using pristine BR than that for electrodes using vulcanized BR is highlighted in the rectangle.

to understand the performance differences depending on the operational pressure, as illustrated in Fig. 3e. Any contribution of anodes (counter electrodes) could be ruled out by using "zero-strain" $Li_4Ti_5O_{12}$ (LTO, volumetric strain of ~0.2%) [28]. The first-cycle charge–discharge voltage profiles of the NCM/LTO all-solid-state cells and the corresponding pressure changes are plotted in Fig. 3f. The overall pressure change shapes were consistent with the lattice volume changes of the Ni-rich layered oxides upon (de)lithiation [29,38]. Importantly, at the end of discharge, the cells using pristine BR, despite the lower depth of discharge, showed a higher pressure value than those using vulcanized BR (outlined by a rectangle in red, Fig. 3f). The higher terminal pressure reflects the formation of larger amounts of cracks and/or void spaces created by the electrochemo-mechanical degradation [38].

The microstructural evolution of the NCM electrodes using pristine and vulcanized (S2) BR after the first charge and discharge was examined using cross-sectional FESEM-BSE measurements, as shown in Fig. 4. After the first charge (and subsequent discharge), cracks occurred at the NCM–LPSX interfaces in the electrode layer (referred to as the "bulk" region) and at the interfaces between the electrode and the SE layers (referred to as the "interface" region). The area fraction of the cracks at the bulk and interface regions was then quantified, and the results are shown in Fig. 4g–l (a typical analysis image is shown in Fig. S12 and detailed values are summarized in Table S2) [29]. The area fraction of the cracks increased significantly after the first charge in both the bulk and interface regions. Importantly, the area fraction of the cracks in the interface region was higher for the electrodes using pristine BR than for the electrodes using vulcanized BR (Fig. 4k), which was also revealed by a delamination between the NCM electrode and the SE layers (Fig. 4b). After the first discharge, the average area fraction of the cracks in the interface region also showed slightly higher values for the electrodes using pristine BR than for the electrodes using vulcanized BR. However, in the bulk region, both after the first charge and discharge, the area fraction of the cracks showed similar values. These results indicate that the delamination between the NCM electrodes and the SE layers has a more dominant effect on the electrochemo-mechanical degradation than the contact loss occurring at the NCM–SE interfaces in the electrode layers.

From the results of operando electrochemical pressiometry (Fig. 3) and cross-sectional FESEM-BSE analyses (Fig. 4), the degradation mechanism varied with the use of vulcanized binders, as illustrated in Fig. 5. The mismatch in the volumetric strain during the charge and discharge between the breathing electrode layer and the intact SE layer causes delamination at the interface, which leads to the degradation of the electrochemical performance. The loosened and/or altered interfacial contacts between the solid components at the lower scale should also be an additional factor affecting the electrochemo-mechanical degradation. When linear (pristine) BR binders are used, the components in the electrodes are highly prone to movements driven by mechanical stresses (just slipping). In contrast, when vulcanized BR binders with a scaffolding structure are employed, the highly elastic binders hold particles tightly, thereby maintaining their structural integrity [60].

Finally, 16 × 25 mm^2 pouch-type NCM/LTO full cells were fabricated using pristine or vulcanized (S2) BR for the NCM electrodes, and the results obtained under no external pressure are displayed in Fig. 6. Consistent with the half cell results in Fig. 3, much higher capacities were obtained for the electrodes using vulcanized BR, compared with those for the electrodes using pristine BR (165 vs. 150 mA h g^{-1} and 153 vs. 121 mA h g^{-1} at 0.05C and 0.2C, respectively). The NCM/LTO full cells using vulcanized BR also showed a reasonable cycling performance, as shown in Fig. 6b. The capacity retention for the electrodes using vulcanized BR was 72.8% at the 150th cycle, compared with the capacity at the 2nd cycle, which was higher than that of the electrodes using pristine BR (61.8 %).

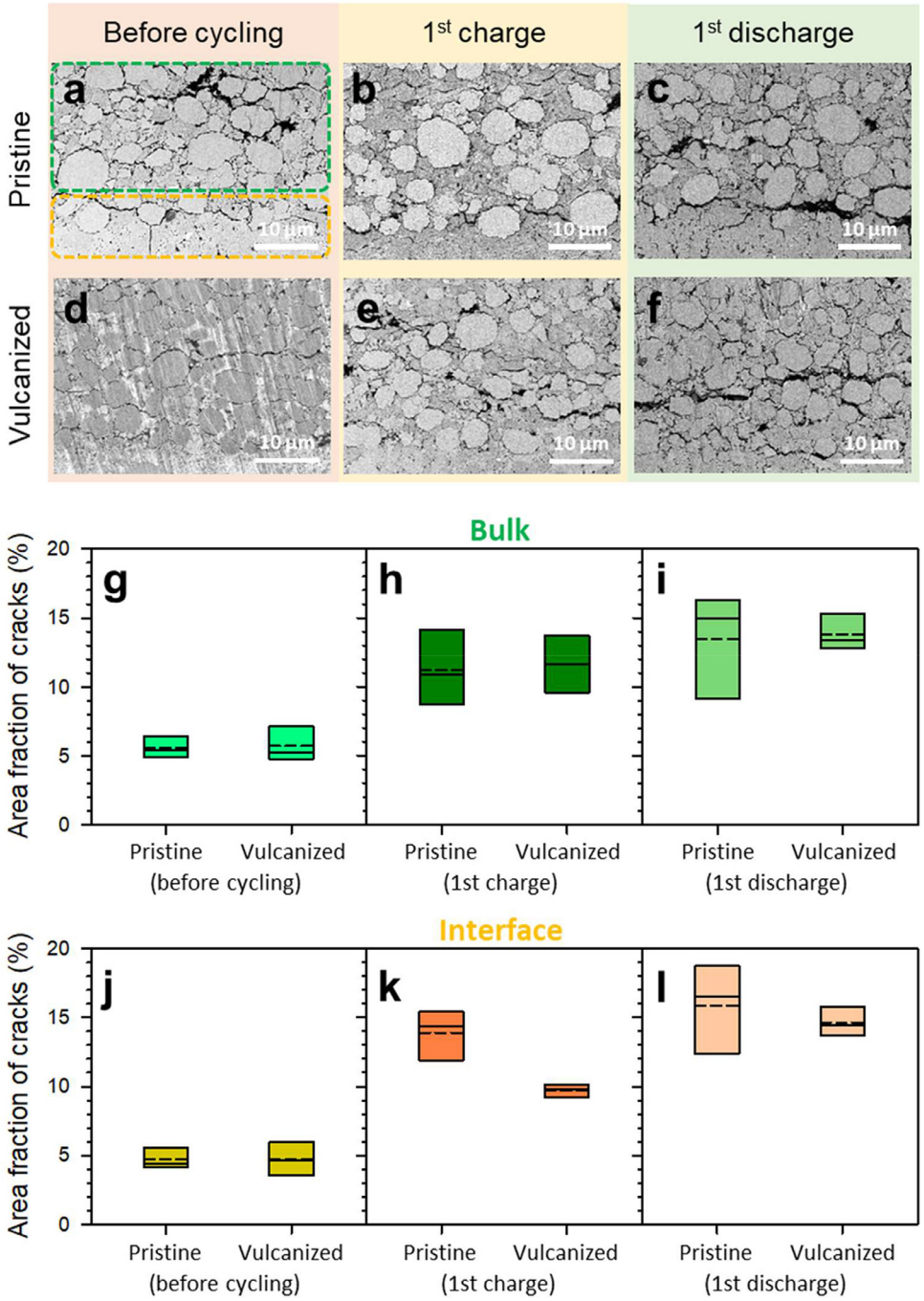

Fig. 4. FESEM-BSE analysis results of NCM electrodes prepared using pristine and vulcanized BR. (a) Cross-sectional FESEM-BSE images for electrodes using a–c) pristine BR and (d–f) vulcanized BR (d–f) before cycling, after the first charge to 4.3 V (vs. Li/Li^+), and after the subsequent discharge to 3.0 V (vs. Li/Li^+). In (a), the bulk and interface regions used for quantitative analysis are outlined in green and yellow, respectively. Box plots of the area fraction of the cracks of the NCM electrodes for g–i) bulk and j–l) interface regions before cycling, after the first charge to 4.3 V (vs Li/Li^+), and the subsequent discharge to 3.0 V (vs Li/Li^+). The median and mean values are indicated as solid and dotted horizontal lines, respectively. The analysis results are summarized in Table S2 in the Supporting Information.

3. Conclusions

In summary, a new, simple, and scalable protocol to reinforce binders, that is, *in situ* vulcanization, was successfully developed for practical sulfide-SE-based ASLBs operated under a low external pressure. The vulcanization protocol was integrated into the slurry fabrication process by simply adding sulfur and additives to the slurries. Moreover, the vulcanization conditions to achieve the highest performance were optimized. The use of vulcanized BR for the NCM electrodes did not result in any marked differences in performance, compared with that of the electrodes using pristine BR, under the conventional high pressure of 70 MPa. In contrast, the NCM electrodes tailored using vulcanized BR significantly outperformed those using pristine BR under a practically relevant low pressure of 2 MPa. To the best of our knowledge, this is the first study to report an improved performance of ASLB cells operated under a low external pressure, enabled by tailoring polymeric binders. The results of the operando electrochemical pressiometry and cross-sectional FESEM-BSE analyses demonstrated that the crosslinked network polymers providing the scaffolding structure harnessed the movements of electrode components, thereby restraining the detrimental electrochemo-mechanical effects. Finally, NCM/LTO pouch-type full cells tested under no external pressure confirmed the significant outperformance when using vulcanized BR, compared with the use of pristine BR, which highlights the practicability of our protocol. The issue of the low operating pressure for ASLBs studied herein will motivate considerable interest in materials chemistry and engineering in this field. In addition, we believe that our simple strategy to strengthen the mechanical properties of binders is a breakthrough for practical all-solid-state technology.

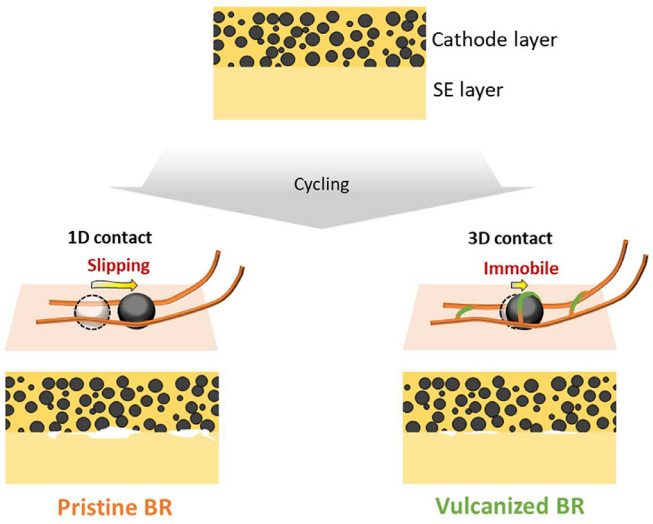

Fig. 5. Schematic illustrating the electrochemo-mechanical effects in NCM electrodes using pristine and vulcanized BR upon cycling. Different responses against mechanical forces for the linear (pristine, left) and crosslinked (right) BR, and the resulting different degrees of degradation are illustrated.

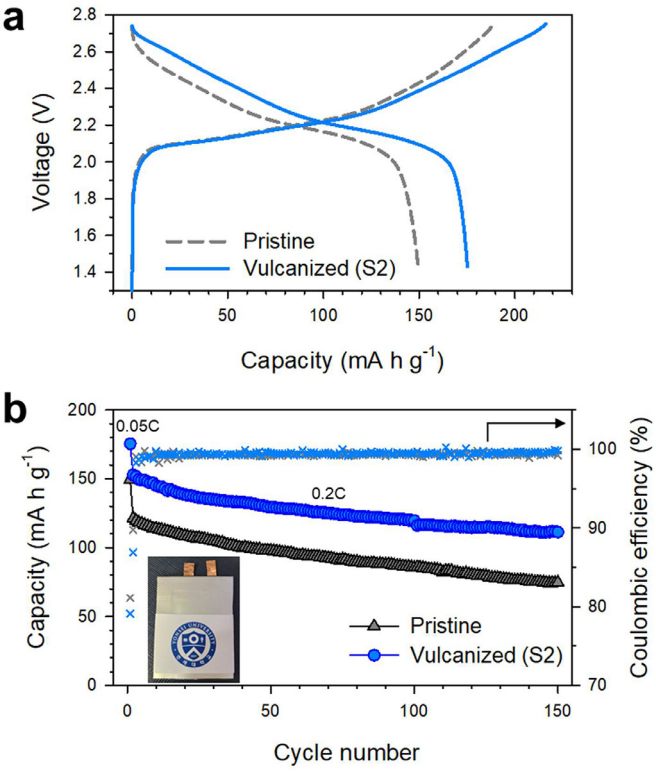

Fig. 6. Electrochemical performance results at 30 °C for NCM/LTO all-solid-state pouch-type full cells employing pristine and vulcanized (S2) BR, operated under no external pressure. (a) First-cycle charge–discharge voltage profiles of the pouch-type full cells at 0.05C and (b) corresponding cycling performances with a photograph of a pouch-type full cell.

4. Experimental section

4.1. Preparation of materials

Argyrodite $Li_6PS_5Cl_{0.5}Br_{0.5}$ (LPSX) was prepared via ball-milling and subsequent heat treatment under an Ar atmosphere. After ball-milling a stoichiometric mixture of Li_2S (99.9%, Alfa Aesar), P_2S_5 (99%, Sigma Aldrich), LiCl (99.99%, Sigma Aldrich), and LiBr (99.99%, anhydrous, Alfa Aesar) at 600 rpm for 10 h in a ZrO_2 vial with ZrO_2 balls using Pulverisette 7PL (Fritsch GmbH), heat treatment was conducted at 550 °C for 5 h under Ar atmosphere. The Li^+ conductivity of the resulting powder was 5.9 mS cm^{-1} at 30 °C. NCM powders coated with $LiNbO_3$ (1.4 wt%) via a wet-chemical method using lithium ethoxide (99.95%, Sigma Aldrich) and niobium ethoxide (99.95%, Sigma Aldrich) were used [40].

4.2. Fabrication of electrodes

For the fabrication of NCM electrodes without vulcanization, wet slurries consisting of NCM, LPSX, polymeric binder (BR), and carbon additive (Super C65) were prepared using butyl butyrate (BB, 99%, TCI Corp.) as the processing solvent with the target compositions. For the fabrication of NCM electrodes with vulcanization, BR/BB solutions were prepared by adding BR, sulfur (99.5%, Alfa Aesar), MBT (2-mercaptobenzothiazole, 97%, Sigma Aldrich), ZnO (< 100 nm particle size, Sigma Aldrich), and stearic acid (SA, 98.5%, Sigma Aldrich) to BB. The weight ratio of BR:sulfur:ZnO:MBT:SA was 100:x:5:4-x:1. Then, the as-prepared BR/BB solutions were added to the slurries consisting of NCM, LPSX, and carbon additives (Super C65) in BB. The NCM electrode composition was 70:27.5:1:1.5 (NCM/LPSX/Super C65/BR). The as-prepared slurry mixtures were cast on current collectors of carbon-coated Al foils using the doctor-blade method, followed by heat treatment under vacuum at 150 °C for 12 h to prepare the NCM electrodes. The solids (BR, sulfur, MBT, ZnO, SA) and liquid (BB) used for slurries were dried using molecular sieves (4 Å, Daejung) and at 100 °C under vacuum, respectively. Mass loadings of the electrodes were ~8 and 4.2 mg_{NCM} cm^{-2} for half cells and full cells, respectively. For the fabrication of LPSX-binder samples with the weight ratio of 55:3 (which was identical to that for the NCM electrodes), wet slurries consisting of LPSX and polymeric binder (S3, S2, S1, BR) were prepared using BB as the processing solvent. The prepared slurry mixtures were cast on glass slides and dried under vacuum at 150 °C for 12 h.

4.3. Material characterization

For XRD measurements, SE or SE–binder samples were hermetically sealed with a beryllium window and mounted on a MiniFlex 600 diffractometer (Rigaku Corp.; Cu K_α radiation of 1.5406 Å) at 40 kV and 15 mA. Raman spectra were collected using a LabRAM ARAMIS (Horiba Jobin Yvon Corp.) with a vis–NIR 514 nm laser. Tensile tests were performed using a μTXA Multi-axis Micro-Texture Analyzer (Yeonjin S-Tech Corp.) with 1 × 3 cm^2 BR film samples. Toughness of binders shown in Fig. 2f was obtained by integrating the stress-strain curves in Fig. 2e. The nanoindentation tests were conducted under a controlled load with a maximum force of 50 μN using a TI 950 (Bruker Corp.). The BR samples used for the nanoindentation tests were prepared on glass slides with a thickness of ~10 μm. Cross-sectioned NCM electrode samples were obtained by polishing with an Ar ion beam at 6 kV for 8 h and subsequently at 4 kV for 2 h (JEOL, IB-19510CP). The polished NCM electrodes were transferred to an FESEM equipment without any exposure to air. The corresponding FESEM-BSE images were obtained using AURIGA (Carl Zeiss). For the TOFSIMS measurements, after NCM electrodes with composition of 70:28.5:1.5 (NCM/LPSX/binder weight ratio) were polished with an Ar ion beam, data were acquired using a TOFSIMS.5 instrument (ION-TOF) equipped with a 30 keV Bi cluster primary-ion gun for analysis. Bi^{3+} ions with an energy of 30 keV were used as primary-ion species, and the 10 × 10 $μm^2$ or 5 × 5 $μm^2$ analysis area were rasterized.

4.4. Electrochemical characterization

Li-In (nominal composition: $Li_{0.5}In$) as the counter and reference electrodes were prepared by ball-milling In (Sigma Aldrich, 99%) and Li (FMC Lithium Corp.) powders. To fabricate the NCM/Li-In half cells or

NCM/LTO full cells, the NCM electrodes and Li-In (or LTO) electrodes were placed on each side of the pre-pelletized LPSX layers (150 mg) and pelletized at 370 MPa and room temperature. The thickness of the LPSX layers was ~600 μm. Galvanostatic charge–discharge cycling tests were conducted at 30 °C or 60 °C between 3.0 and 4.3 V (vs. Li/Li^+) for NCM/Li-In half cells or between 1.43 and 2.75 V for NCM/LTO full cells. All the procedures related to the fabrication of the all-solid-state cells were performed in a polyether ether ketone (PEEK) mold (1.3 cm^2) with two Ti metal rods. For the fabrication of 40 × 50 mm^2 NCM/LTO pouch-type full cells, an LPSX SE film with a thickness of 100 μm was attached to the LTO anode using warm isotatic press (WIP, Ilshinautoclave Corp.). The SE film composition was 97:3 (LPSX/NBR weight ratio). Then, an NCM cathode and the SE film/LTO anode were stacked together, and the whole assembly was sealed using a pouch and pressurized at 375 MPa using WIP.

Declaration of Competing Interest

The authors declare that they have no known competing financial interests or personal relationships that could have appeared to influence the work reported in this paper.

CRediT authorship contribution statement

Tae Young Kwon: Conceptualization, Methodology, Investigation, Writing – original draft. **Kyu Tae Kim:** Methodology, Investigation. **Dae Yang Oh:** Conceptualization. **Yong Bae Song:** Investigation. **Seunggoo Jun:** Investigation. **Yoon Seok Jung:** Conceptualization, Supervision, Writing – review & editing.

Acknowledgments

This work was supported by the Technology Development Program to Solve Climate Changes and by the Basic Science Research Program through the National Research Foundation of Korea (NRF) funded by the Ministry of Science, ICT & Future Planning (NRF-2018R1A2B6004996 and 2017M1A2A2044501), and by the Technology Innovation Program (20007045 and 20012216) funded by the Ministry of Trade, Industry & Energy (MOTIE, Korea). The work was also funded by the Yonsei University Research Fund of 2021 (2021-22-0326).

Supplementary materials

Supplementary material associated with this article can be found, in the online version, at doi:10.1016/j.ensm.2022.04.017.

References

[1] Y. Kato, S. Hori, T. Saito, K. Suzuki, M. Hirayama, A. Mitsui, M. Yonemura, H. Iba, R. Kanno, High-power all-solid-state batteries using sulfide superionic conductors, Nat. Energy 1 (2016) 16030, doi:10.1038/NENERGY.2016.30.

[2] K.H. Park, Q. Bai, D.H. Kim, D.Y. Oh, Y. Zhu, Y. Mo, Y.S. Jung, Design strategies, practical considerations, and new solution processes of sulfide solid electrolytes for all-solid-state batteries, Adv. Energy Mater. 8 (2018) 1800035, doi:10.1002/aenm.201800035.

[3] A. Manthiram, X. Yu, S. Wang, Lithium battery chemistries enabled by solid-state electrolytes, Nat. Rev. Mater. 2 (2017) 16103, doi:10.1038/natrevmats.2016.103.

[4] Z. Zhang, Y. Shao, B. Lotsch, Y.S. Hu, H. Li, J. Janek, L.F. Nazar, C. Nan, J. Maier, M. Armand, L. Chen, New horizons for inorganic solid state ion conductors, Energy Environ. Sci. 11 (2018) 1945–1976, doi:10.1039/C8EE01053F.

[5] T. Famprikis, P. Canepa, J.A. Dawson, M.S. Islam, C. Masquelier, Fundamentals of inorganic solid-state electrolytes for batteries, Nat. Mater. 18 (2019) 1278–1291, doi:10.1038/s41563-019-0431-3.

[6] F. Han, A.S. Westover, J. Yue, X. Fan, F. Wang, M. Chi, D.N. Leonard, N.J. Dudney, H. Wang, C. Wang, High electronic conductivity as the origin of lithium dendrite formation within solid electrolytes, Nat. Energy 4 (2019) 187–196, doi:10.1038/s41560-018-0312-z.

[7] R. Chen, Q. Li, X. Yu, L. Chen, H. Li, Approaching practically accessible solid-state batteries: stability issues related to solid electrolytes and interfaces, Chem. Rev. 120 (2020) 6820–6877, doi:10.1021/acs.chemrev.9b00268.

[8] Y.G. Lee, S. Fujiki, C. Jung, N. Suzuki, N. Yashiro, R. Omoda, D.S. Ko, T. Shiratsuchi, T. Sugimoto, S. Ryu, J.H. Ku, T. Watanabe, Y. Park, Y. Aihara, D. Im, I.T. Han, High-energy long-cycling all-solid-state lithium metal batteries enabled by silver–carbon composite anodes, Nat. Energy 5 (2020) 299–308, doi:10.1038/s41560-020-0575-z.

[9] J. Wu, S. Liu, F. Han, X. Yao, C. Wang, Lithium/sulfide all-solid-state batteries using sulfide electrolytes, Adv. Mater. 33 (2021) 2000751, doi:10.1002/adma.202000751.

[10] J. Wu, L. Shen, Z. Zhang, G. Liu, Z. Wang, D. Zhou, H. Wan, X. Xu, X. Yao, All-solid-state lithium batteries with sulfide electrolytes and oxide cathodes, Electrochem. Energy Rev. 4 (2021) 101–135, doi:10.1007/s41918-020-00081-4.

[11] H.J. Deiseroth, S.T. Kong, H. Eckert, J. Vannahme, C. Reiner, T. Zaiss, M. Schlosser, Li_6PS_5X: a class of crystalline Li-rich solids with an unusually high Li^+ mobility, Angew. Chem. Int. Ed. 47 (2008) 755–758, doi:10.1002/anie.200703900.

[12] R. Murugan, V. Thangadurai, W. Weppner, Fast lithium ion conduction in garnet-type Li7La3Zr2O12, Angew. Chem. Int. Ed. 46 (2007) 7778–7781, doi:10.1002/anie.200701144.

[13] T. Asano, A. Sakai, S. Ouchi, M. Sakaida, A. Miyazaki, S. Hasegawa, Solid halide electrolytes with high lithium-ion conductivity for application in 4 V class bulk-type all-solid-state batteries, Adv. Mater. 30 (2018) e1803075, doi:10.1002/adma.201803075.

[14] H. Kwak, D. Han, J. Lyoo, J. Park, S.H. Jung, Y. Han, G. Kwon, H. Kim, S.T. Hong, K.W. Nam, Y.S. Jung, New cost-effective halide solid electrolytes for all-solid-state batteries: mechanochemically prepared Fe^{3+}-substituted Li_2ZrCl_6, Adv. Energy Mater. 11 (2021) 2003190, doi:10.1002/aenm.202003190.

[15] J.W. Choi, D. Aurbach, Promise and reality of post-lithium-ion batteries with high energy densities, Nat. Rev. Mater. 1 (2016) 1, doi:10.1038/natrevmats.2016.13.

[16] K. Liu, Y.Y. Liu, D.C. Lin, A. Pei, Y. Cui, Materials for lithium-ion battery safety, Sci. Adv. 4 (2018) eaas9820, doi:10.1126/sciadv.aas9820.

[17] D.H.S. Tan, Y.T. Chen, H. Yang, W. Bao, B. Sreenarayanan, J.M. Doux, W. Li, B. Lu, S.Y. Ham, B. Sayahpour, J. Scharf, E.A. Wu, G. Deysher, H.E. Han, H.J. Hah, H. Jeong, J.B. Lee, Z. Chen, Y.S. Meng, Carbon-free high-loading silicon anodes enabled by sulfide solid electrolytes, Science 373 (2021) 1494–1499, doi:10.1126/science.abg7217.

[18] J. Lee, K. Lee, T. Lee, H. Kim, K. Kim, W. Cho, A. Coskun, K. Char, J.W. Choi, *In situ* deprotection of polymeric binders for solution-processible sulfide-based all-solid-state batteries, Adv. Mater. 32 (2020) 2001702, doi:10.1002/adma.202001702.

[19] T. Ates, M. Keller, J. Kulisch, T. Adermann, S. Passerini, Development of an all-solid-state lithium battery by slurry-coating procedures using a sulfidic electrolyte, Energy Storage Mater. 17 (2019) 204–210, doi:10.1016/j.ensm.2018.11.011.

[20] A. Sakuda, K. Kuratani, M. Yamamoto, M. Takahashi, T. Takeuchi, H. Kobayashi, All-solid-state battery electrode sheets prepared by a slurry coating process, J. Electrochem. Soc. 164 (2017) A2474–A2478, doi:10.1149/2.0951712jes.

[21] D. Cao, Q. Li, X. Sun, Y. Wang, X. Zhao, E. Cakmak, W. Liang, A. Anderson, S. Ozcan, H. Zhu, Amphipathic binder integrating ultrathin and highly ion-conductive sulfide membrane for cell-level high-energy-density all-solid-state batteries, Adv. Mater. 33 (2021) 2105505, doi:10.1002/adma.202105505.

[22] D.H. Kim, H.A. Lee, Y.B. Song, J.W. Park, S.M. Lee, Y.S. Jung, Sheet-type Li_6PS_5Cl-infiltrated Si anodes fabricated by solution process for all-solid-state lithium-ion batteries, J. Power Sources 426 (2019) 143–150, doi:10.1016/j.jpowsour.2019.04.028.

[23] D.Y. Oh, Y.J. Nam, K.H. Park, S.H. Jung, K.T. Kim, A.R. Ha, Y.S. Jung, Slurry-fabricable Li^+-conductive polymeric binders for practical all-solid-state lithium-ion batteries enabled by solvate ionic liquids, Adv. Energy Mater. 9 (2019) 1802927, doi:10.1002/aenm.201802927.

[24] J.M. Doux, Y. Yang, D.H.S. Tan, H. Nguyen, E.A. Wu, X. Wang, A. Banerjee, Y.S. Meng, Pressure effects on sulfide electrolytes for all solid-state batteries, J. Mater. Chem. A 8 (2020) 5049–5055, doi:10.1039/C9TA12889A.

[25] Y. Tang, L. Zhang, J. Chen, H. Sun, T. Yang, Q. Liu, Q. Huang, T. Zhu, J. Huang, Electro-chemo-mechanics of lithium in solid state lithium metal batteries, Energy Environ. Sci. 14 (2021) 602–642, doi:10.1039/D0EE02525A.

[26] R. Koerver, W. Zhang, L.d. Biasi, S. Schweidler, A.O. Kondrakov, S. Kolling, T. Brezesinski, P. Hartmann, W.G. Zeier, J. Janek, Chemo-mechanical expansion of lithium electrode materials – on the route to mechanically optimized all-solid-state batteries, Energy Environ. Sci. 11 (2018) 2142–2158, doi:10.1039/C8EE00907D.

[27] F.P. McGrogan, T. Swamy, S.R. Bishop, E. Eggleton, L. Porz, X. Chen, Y.M. Chiang, K.J.V. Vliet, Compliant yet brittle mechanical behavior of Li_2S–P_2S_5 lithium-ion-conducting solid electrolyte, Adv. Energy Mater. 7 (2017) 1602011, doi:10.1002/aenm.201602011.

[28] S. Jun, Y.J. Nam, H. Kwak, K.T. Kim, D.Y. Oh, Y.S. Jung, Operando differential electrochemical pressiometry for probing electrochemo-mechanics in all-solid-state batteries, Adv. Funct. Mater. 30 (2020) 2002535, doi:10.1002/adfm.202002535.

[29] Y. Han, S.H. Jung, H. Kwak, S. Jun, H.H. Kwak, J.H. Lee, S.T. Hong, Y.S. Jung, Single- or poly-crystalline ni-rich layered cathode, sulfide or halide solid electrolyte: which will be the winners for all-solid-state batteries? Adv. Energy Mater. 11 (2021) 2100126, doi:10.1002/aenm.202100126.

[30] M.J. Wang, E. Kazyak, N.P. Dasgupta, J. Sakamoto, Transitioning solid-state batteries from lab to market: linking electro-chemo-mechanics with practical considerations, Joule 5 (2021) 1371–1390, doi:10.1016/j.joule.2021.04.001.

[31] J. Kasemchainan, S. Zekoll, D.S Jolly, Z. Ning, G.O. Hartley, J. Marrow, P.G. Bruce, Critical stripping current leads to dendrite formation on plating in lithium anode solid electrolyte cells, Nat. Mater. 18 (2019) 1105–1111, doi:10.1038/s41563-019-0438-9.

[32] T. Shi, Y.Q. Zhang, Q. Tu, Y. Wang, M.C. Scott, G. Ceder, Characterization of mechanical degradation in an all-solid-state battery cathode, J. Mater. Chem. 8 (2020) 17399–17404, doi:10.1039/D0TA06985J.

[33] J.A. Lewis, F.J.Q. Cortes, Y. Liu, J.C. Miers, A. Verma, B.S. Vishnugopi, J. Tippens, D. Prakash, T.S. Marchese, S.Y. Han, C. Lee, P.P. Shetty, H.W. Lee, P. Shevchenko, F.D. Carlo, C. Saldana, P.P. Mukherjee, M.T. McDowell, Linking void and interphase evolution to electrochemistry in solid-state batteries using operando X-ray tomography, Nat. Mater. 20 (2021) 503–510, doi:10.1038/s41563-020-00903-2.

[34] Y.B. Song, H. Kwak, W. Cho, K.S. Kim, Y.S. Jung, K.H. Park, Electrochemo-mechanical effects as a critical design factor for all-solid-state batteries, Curr. Opin. Solid State Mater. Sci. 26 (2022) 100977, doi:10.1016/j.cossms.2021.100977.

[35] Q. Zhang, H. Wan, G. Liu, Z. Ding, J.P. Mwizerwa, X. Yao, Rational design of multi-channel continuous electronic/ionic conductive networks for room temperature vanadium tetrasulfide-based all-solid-state lithium-sulfur batteries, Nano Energy 57 (2019) 771–782, doi:10.1016/j.nanoen.2019.01.004.

[36] H. Wan, L. Cai, F. Han, J.P. Mwizerwa, C. Wang, X. Yao, Construction of 3D electronic/ionic conduction networks for all-solid-state lithium batteries, Small 15 (2019) 1905849, doi:10.1002/smll.201905849.

[37] R. Koerver, I. Aygün, T. Leichtweiß, C. Dietrich, W. Zhang, J.O. Binder, P. Hartmann, W.G. Zeier, J. Janek, Capacity fade in solid-state batteries: interphase formation and chemomechanical processes in nickel-rich layered oxide cathodes and lithium thiophosphate solid electrolytes, Chem. Mater. 29 (2017) 5574–5582, doi:10.1021/acs.chemmater.7b00931.

[38] S.H. Jung, U.H. Kim, J.H. Kim, S. Jun, C.S. Yoon, Y.S. Jung, Y.K. Sun, Ni-rich layered cathode materials with electrochemo-mechanically compliant microstructures for all-solid-state Li batteries, Adv. Energy Mater. 10 (2020) 1903360, doi:10.1002/aenm.201903360.

[39] A. Banerjee, X. Wang, C. Fang, E.A. Wu, Y.S. Meng, Interfaces and interphases in all-solid-state batteries with inorganic solid electrolytes, Chem. Rev. 120 (2020) 6878–6933, doi:10.1021/acs.chemrev.0c00101.

[40] D.H. Kim, D.Y. Oh, K.H. Park, Y.E. Choi, Y.J. Nam, H.A. Lee, S.M. Lee, Y.S. Jung, Infiltration of solution-processable solid electrolytes into conventional Li-ion-battery electrodes for all-solid-state Li-ion batteries, Nano Lett. 17 (2017) 3013–3020, doi:10.1021/acs.nanolett.7b00330.

[41] Y.J. Nam, D.Y. Oh, S.H. Jung, Y.S. Jung, Toward practical all-solid-state lithium-ion batteries with high energy density and safety: comparative study for electrodes fabricated by dry- and slurry-mixing processes, J. Power Sources 375 (2018) 93–101, doi:10.1016/j.jpowsour.2017.11.031.

[42] M. Yamamoto, Y. Terauchi, A. Sakuda, M. Takahashi, Slurry mixing for fabricating silicon-composite electrodes in all-solid-state batteries with high areal capacity and cycling stability, J. Power Sources 402 (2018) 506–512, doi:10.1016/j.jpowsour.2018.09.070.

[43] N.A. Dunlap, J. Kim, K.H. Oh, S.H. Lee, Slurry-coated sheet-style Sn-PAN anodes for all-solid-state Li-ion batteries, J. Electrochem. Soc. 166 (2019) A915–A922, doi:10.1149/2.0151906jes.

[44] D.H. Kim, Y.H. Lee, Y.B. Song, H. Kwak, S.Y. Lee, Y.S. Jung, Thin and flexible solid electrolyte membranes with ultrahigh thermal stability derived from solution-processable Li argyrodites for all-solid-state Li-ion batteries, ACS Energy Lett. 5 (2020) 718–727, doi:10.1021/acsenergylett.0c00251.

[45] J. Schnell, T. Gunther, T. Knoche, C. Vieider, L. Kohler, A. Just, M. Keller, S. Passerini, G. Reinhart, All-solid-state lithium-ion and lithium metal batteries - paving the way to large-scale production, J. Power Sources 382 (2018) 160–175, doi:10.1016/j.jpowsour.2018.02.062.

[46] K.T. Kim, D.Y. Oh, S. Jun, Y.B. Song, T.Y. Kwon, Y. Han, Y.S. Jung, Tailoring slurries using cosolvents and Li salt targeting practical all-solid-state batteries employing sulfide solid electrolytes, Adv. Energy Mater. 11 (2021) 2003766, doi:10.1002/aenm.202003766.

[47] D.Y. Oh, K.T. Kim, S.H. Jung, D.H. Kim, S. Jun, S. Jeoung, H.R. Moon, Y.S. Jung, Tactical hybrids of Li^+-conductive dry polymer electrolytes with sulfide solid electrolytes: toward practical all-solid-state batteries with wider temperature operability, Mater. Today (2022), doi:10.1016/j.mattod.2021.01.006.

[48] H. Yuan, H.X. Nan, C.Z. Zhao, G.L. Zhu, Y. Lu, X.B. Cheng, Q.B. Liu, C.X. He, J.Q. Huang, Q. Zhang, Slurry-coated sulfur/sulfide cathode with Li metal anode for all-solid-state lithium-sulfur pouch cells, Batter. Supercaps 3 (2020) 596–603, doi:10.1002/batt.202000051.

[49] B. Koo, H. Kim, Y. Cho, K.T. Lee, N.S. Choi, J. Cho, A highly cross-linked polymeric binder for high-performance silicon negative electrodes in lithium ion batteries, Angew. Chem. Int. Ed. 51 (2012) 8762–8767, doi:10.1002/anie.201201568.

[50] S. Choi, T.w. Kwon, A. Coskun, J.W. Choi, Highly elastic binders integrating polyrotaxanes for silicon microparticle anodes in lithium ion batteries, Science 357 (2017) 279–283, doi:10.1126/science.aal4373.

[51] N.C. Rosero-Navarro, T. Kinoshita, A. Miura, M. Higuchi, K. Tadanaga, Effect of the binder content on the electrochemical performance of composite cathode using Li_6PS_5Cl precursor solution in an all-solid-state lithium battery, Ionics 23 (2017) 1619–1624, doi:10.1007/s11581-017-2106-x.

[52] J. Lee, T. Lee, K. Char, K.J. Kim, J.W. Choi, Issues and advances in scaling up sulfide-based all-solid-state batteries, Acc. Chem. Res. 54 (2021) 3390–3402, doi:10.1021/acs.accounts.1c00333.

[53] D.A. Boyd, Sulfur and its role in modern materials science, Angew. Chem. Int. Ed. 55 (2016) 15486–15502, doi:10.1002/anie.201604615.

[54] M. Nasir, G.K. Teh, The effects of various types of crosslinks on the physical properties of natural rubber, Eur. Polym. J. 24 (1988) 733–736, doi:10.1016/0014-3057(88)90007-9.

[55] R.P. Wool, R.P Wool, X.S. Sun, in: Bio-Based Polymers and Composites, Academic Press, Burlington, 2005, pp. 202–255.

[56] P.J. Flory, Statistical mechanics of swelling of network structures, J. Chem. Phys. 18 (1950) 108–111, doi:10.1063/1.1747424.

[57] J.L. Koenig, M.M. Coleman, J.R. Shelton, P.H. Starmer, Raman spectrographic studies of the vulcanization of rubbers. I. Raman spectra of vulcanized rubbers, Rubber Chem. Technol. 44 (1971) 71–86, doi:10.5254/1.3547368.

[58] T. Liu, Q. Chu, C. Yan, S. Zhang, Z. Lin, J. Lu, Interweaving 3D network binder for high-areal-capacity Si anode through combined hard and soft polymers, Adv. Energy Mater. 9 (2019) 1802645, doi:10.1002/aenm.201802645.

[59] G. Yoo, S. Kim, C. Chanthad, M. Cho, Y. Lee, Elastic rubber-containing multifunctional binder for advanced Li-S batteries, Chem. Eng. J. 405 (2021) 126628, doi:10.1016/j.cej.2020.126628.

[60] S. Kienle, M. Gallei, H. Yu, B. Zhang, S. Krysiak, B.N. Balzer, M. Rehahn, A.D. Schlüter, T. Hugel, Effect of molecular architecture on single polymer adhesion, Langmuir 30 (2014) 4351–4357, doi:10.1021/la500783n.